SLAC-PUB-5791
March 1992
(E/A)

# EXPERIMENTAL CHALLENGES AT LINEAR COLLIDERS*

D. L. BURKE

*Stanford Linear Accelerator Center, Stanford University, Stanford, CA 94309, USA*

## Abstract

**Experience with the operation of detectors at the SLC, and challenges to experimentation at future linear colliders are discussed.**

## 1. General Considerations

### *1.1. The Physics Environment at Future Colliders*

Experimental studies at $e^+e^-$ colliders over the past two decades have provided many key observations and insights to the nature of the fundamental particles and interactions of the Standard Model. Electron-positron collisions are observed to yield events with simple and transparent structures. Annihilation events carry the full energy of the beam, and produce final states that are usually two-jet-like and almost always highly planar. Searches for new phenomena give complete and unambiguous results, and precision studies of strong and electroweak interactions are made with a minimum of bias and background. The physics environment at higher energies will continue to be as ideally suited to the exploration of particle physics.

The Standard Model processes that will predominate at future machines are summarized in Table I. Examples of some of these are shown in Figs. 1 and 2 as they would appear in a typical detector. It is easy to sort the structure of these events by inspection, and with computer reconstruction, the 50 or so pions, kaons, and photons

**Table I.** $e^+e^-$ Annihilation at $E_{cm}$ = 500 GeV.

| Final State | Cross Section ($R^{(a)}$) | Events/(10 $fb^{-1}$) |
|---|---|---|
| QCD (*udscb*) | 9 | 31,000 |
| $W^+W^-$ | 20 | 70,000 |
| $Z^0Z^0$ | 1.2 | 4,200 |
| $t\bar{t}$ ($m_t$ = 150 GeV) | 1 | 3,400 |

(a) $R \equiv 87\ fb/E^2_{cm}$, where $E_{cm}$ is the $e^+e^-$ center-of-mass energy in TeV.

* Work supported by Department of Energy contract DE–AC03–76SF00515.

*Presented at the Workshop on Physics and Experiments with Linear Colliders, Saariselkä, Finland, September 9–14, 1991*

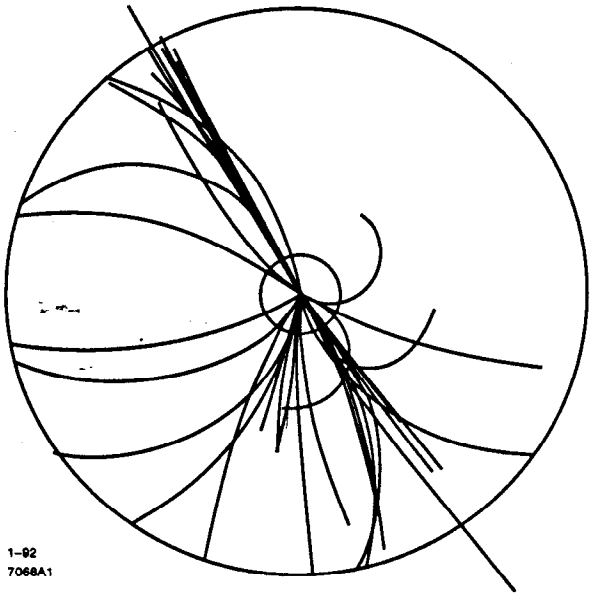


**Figure 1.** Transverse projection of charged tracks produced by the reaction $e^+e^- \to b\bar{b}g$. The particles are shown traversing a volume with outer radius of 1 m which is immersed in a 1 T solenoidal field.

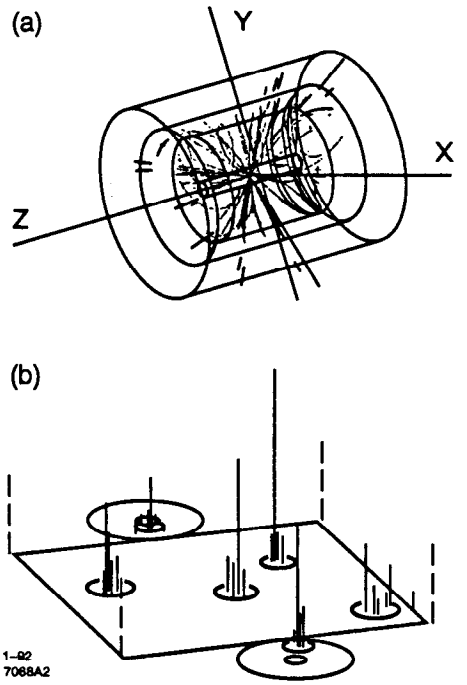


**Figure 2.** Detector views of particles created in the reaction $e^+e^- \to t\bar{t} \to WbWb$. (a) Three dimensional view of charged tracks and electromagnetic showers. (b) Unfolded "Leggo-Plot" of the observed flow of energy in the event.

that appear in the detector can be reduced to a few 4-vectors that accurately describe the underlying partons produced in the annihilation.

### *1.2. Detectors at Future Machines*

Reactions that illustrate the capabilities needed in detectors at high energy linear colliders are given in Table II. Analysis of these events requires good tracking of high-momentum leptons and good reconstruction of quark jets. Isolation of heavy quarks with precision vertex detectors is a powerful tool that must be exploited to make full use of the simplicity of the final states. Measurement of the acollinearity of small-angle Bhabha scatters is necessary to monitor the luminosity of the data sample, and more importantly, to determine the exact energy spectra of the $e^+e^-$ collisions.

Most studies, including those presented at this conference, have used Monte Carlo simulations of detectors with capabilities that have already been achieved at LEP and SLC. For example, the "Standard Detector" of the European study groups[1]

**Table II.** Some experimental targets at $E_{cm} = 500$ GeV.

| Final State | Signature Topology | Required Measurement |
|---|---|---|
| $t\bar{t} \to WbWb$ | 6 jets | $b$-tagging |
| | 4 jets + $l\nu$ | $p_l \sim 50$ GeV |
| $W^+W^-$ | 2 jets + $l\nu$ | $p_l \sim 100$ GeV |
| | | $\theta_{jj} \sim m_W/E_b \approx 15°$ |
| $Z^0H^0$ | $f\bar{f}b\bar{b}$ | flavor-tagging |
| | $f\bar{f}c\bar{c}$ | |
| $e^+e^-$ $(\gamma)$ | low-angle Bhabha | $\theta_{e\pm} > 10°$ |

**Table III.** "Standard detector" parameters.

| | |
|---|---|
| Calorimetery | |
| Resolution (electromagnetic) | $8\% \cdot \sqrt{E} \oplus 2\%$ |
| Resolution (hadronic) | $60\% \cdot \sqrt{E} \oplus 2\%$ |
| Cell size (electromagnetic) | $2°$ |
| Cell size (hadronic) | $4°$ |
| Tracking | |
| Resolution ($p_t$) | $10^{-3} \cdot p_t^2$ |
| Vertex resolution (impact) | $(20\ \mu m)^2 \oplus \left(100\ \mu m/p\right)^2$ |
| Hermiticity | |
| Calorimetery and tracking | $\theta_{e\pm} > 10°$ |

is assumed to provide charged-particle tracking and electromagnetic and hadronic calorimetery that does not extend any technology beyond that now in existence (see Table III). Shown in Fig. 3 are the masses in opposite thrust hemispheres of Standard Model $e^+e^-$ annihilation events (Table I) as they would be reconstructed[2] in such a detector. Only simple cuts on total energy and thrust direction were made to select events for this figure. The peak at the $W$ mass stands out clearly above the background from $q\bar{q}$ production; the size of this peak reflects both the large cross-section for $W$-pair production at high energy and the ease of reconstructing the $W$ decay products accurately.

It is important that even particles that go unseen in the detector, such as neutrinos and beamstrahlung photons, can be fully reconstructed in many instances by applying

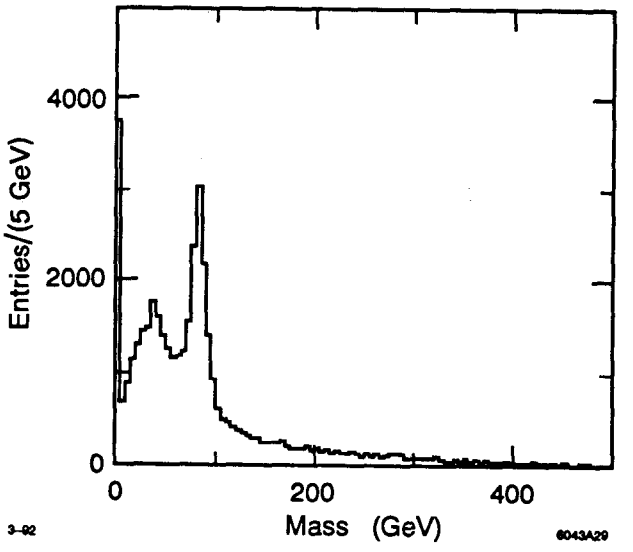


**Figure 3.** Invariant masses in the forward and backward thrust hemispheres of standard model processes reconstructed at a 1 TeV $e^+e^-$ collider.

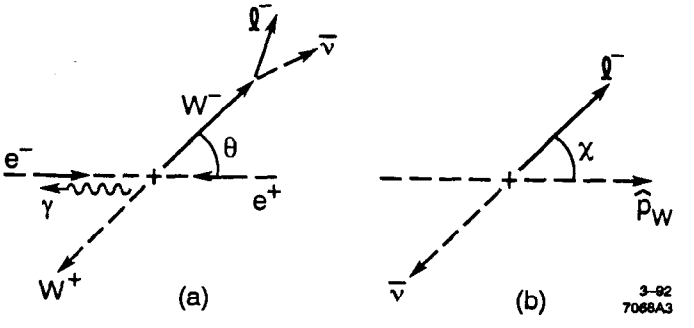


**Figure 4.** Production and decay of $W$-boson pairs in $e^+e^-$ annihilation. The photon shown in the figure may be due either to initial-state radiation or beamstrahlung, and may carry significant energy, but can be safely assumed to propagate along the beamline. The charge of the observed lepton uniquely identifies the charge of the parent boson.

energy-momentum and mass constraints. Such a case is illustrated in Fig. 4. The unknown three-momentum of the neutrino and the energy of a beamstrahlung photon that might appear in the production and decay of $W$ bosons are four quantities that can be reconstructed from measurements made by a suitable detector and the application of six constraints from overall energy-momentum conservation and the known mass of the $W$ boson. This can be done[3] with extremely good accuracy (Fig. 5).

We can anticipate that improvements in the techniques and technologies used in the design and construction of particle detectors will occur. At center of mass energies of several hundred GeV, most applications of electromagnetic and hadronic calorimetery do not suffer from lack of shower statistics, but it is increasingly important to minimize systematic errors in reconstruction of the energies and positions of neutral

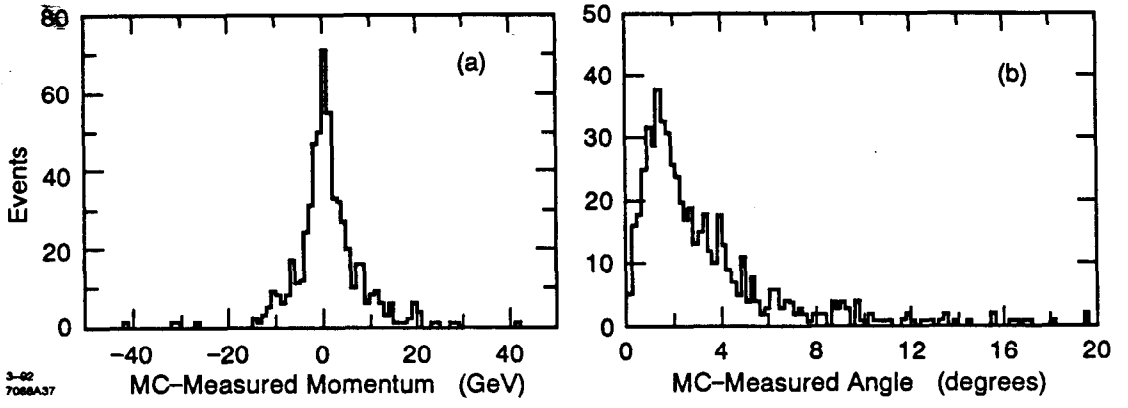


**Figure 5.** The momentum of the parent $W$ boson as reconstructed by a kinematic fit to the hypothesis shown in Fig. 4. See text for discussion of the properties of the detector that were simulated for this study.

**Table IV.** "Improved detector" parameters.

| | |
|---|---|
| Calorimetery | |
| Resolution (electromagnetic) | $8\% \cdot \sqrt{E} \oplus 1\%$ |
| Resolution (hadronic) | $35\% \cdot \sqrt{E} \oplus 2\%$ |
| Cell size (electromagnetic) | $1^\circ$ |
| Cell size (hadronic) | $2^\circ$ |
| Tracking | |
| Resolution ($p_t$) | $2 \times 10^{-4} \cdot p_t^2$ |
| Vertex resolution (impact) | $(5\ \mu m)^2 \oplus \left(50\ \mu m/p\right)^2$ |
| Hermiticity | |
| Calorimetery and tracking | $\theta_{e^\pm} > 10^\circ$ |

hadrons and photons. Charged particles of most interest are similarly energetic, so that scattering of tracks in material of the detector becomes less problematic. It becomes correspondingly more important to measure tracks often and with good resolution. The more aggressive set of goals shown in Table IV might be realizable and certainly would enhance the physics output of the experiment. More systematic and quantitative study is needed to arrive at a complete set of design parameters, but it is clear that existing detectors are not far from ideal.

**Table V.** Photon-photon reactions at $E_{cm} = 1$ TeV.

| Final State | Approximate Total Cross Section |
|---|---|
| $eeee$ | $10^{-26}$ cm$^{-2}$ |
| $ee\mu\mu$ | $3 \times 10^{-31}$ cm$^{-2}$ |
| $eeq\bar{q}$ (Born) | $10^{-31}$ cm$^{-2}$ |
| $ee$ hadrons (VMD) | $10^{-30}$ cm$^{-2}$ |

### *1.3. Event Rates at Linear Colliders*

The total $e^+e^-$ annihilation cross section at high energies is approximately 30 units of $R$ (Table I), or $10^{-35}$ cm$^2$ at 500 GeV. Machine luminosities typically are $10^{33}$ cm$^{-2}$ s$^{-1}$, with an interesting event being produced about once every minute. There are, however, low-energy peripheral two-photon reactions that occur with considerably higher cross sections (Table V). The event rate for these reactions can be quite large, and with some machine designs, it may even be that more than one event occurs *on each machine pulse.*

The luminosity per bunch crossing and the time interval between crossings varies considerably from one machine design to another. Designs based on superconducting linacs yield the lowest luminosity per crossing and the longest spacing between bunches,[4] while machines that utilize linacs with high frequency rf create brighter collisions in short bursts or bunch trains. A typical X-Band (10–15 GHz) linac, for example, will produce 200–300 rf pulses per second and will accelerate 10–20 bunches per pulse; the individual bunches will be spaced by a few nanoseconds.[5,6] In this case, the luminosity delivered by each bunch-bunch interaction will approach $10^{30}$ cm$^{-2}$, and if the detector is unable to resolve the bunch spacing, then the effective luminosity per machine pulse could become an order of magnitude greater.

The beam electrons that recoil from two-photon reactions are rarely scattered to large polar angles, and the particles produced in the $\gamma\gamma$ collision generally form a final state of very low invariant mass, so it will not be difficult to design triggers to select machine pulses on which an interesting annihilation event has occured. But if the detector is unable to assign a particular bunch to each observed secondary particle, then the overlap of these less interesting events with true annihilation events might interfere with analysis of some final states. Detectors can be designed with this capability; it some cases it might require the addition of special hardware to accomplish this task, but given the scope of the machine project, this should not be a restriction. An example[7] of the timing resolution provided by an existing drift chamber is shown in Fig. 6. It should be possible[7] to reconstruct the time of origin of each track with reasonably good accuracy (approximately 1 ns) in a properly designed

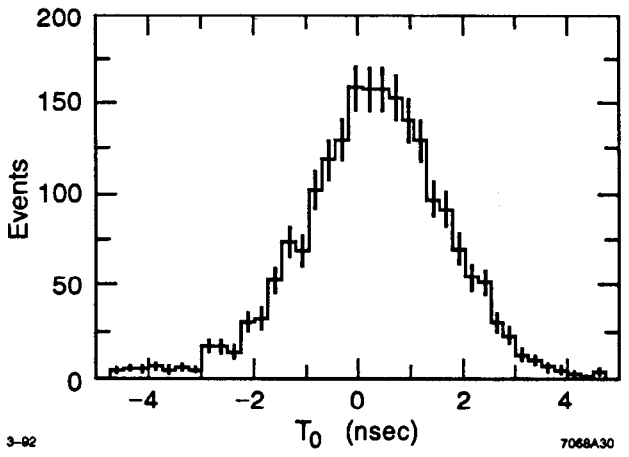


**Figure 6.** Time of origin of tracks observed in the Mark II central drift chamber. The tracks were created in decays of the $Z^0$ at the SLC.

chamber. The need for this accuracy will have to be matched to the bunch crossing rate of the machine.

### *1.4. Beamstrahlung*

Another property of high-energy linear colliders that will be discussed more thoroughly below, is that of "beamstrahlung"—the radiation emitted by beam particles as they pass through the electromagnetic field of the opposing bunch. Corrections for the effects of initial-state radiation in $e^+e^-$ collisions has long been a well-understood process, and similar techniques will be needed at future colliders to account for the smearing of annihilation center of mass energies by beamstrahlung. Examples[8] of the spectra of center of mass energies at various machines are shown in Fig. 7. The effect of initial-state radiation, which is roughly comparable, is also shown.

The consequences of these effects on the analysis of data have been reported by several groups at the 1991 Workshop on Physics and Experiments with Linear Colliders, and techniques to correct data, and even individual events, for radiation of energy by the incident particles prior to collision have been developed. It is extremely rare that more than one hard photon is emitted in any event, and those that are radiated travel along the incident beam direction,[8] so it is often possible to simply include the radiation as an unknown parameter in a likelihood fit to the event topology. This works well for analyses of exclusive final states such as $W^+W^-$ and $t\bar{t}$ pairs. More generally it is necessary to reconstruct the spectrum of collisions that occur in any given data sample. It has been shown[9] that a good image of this spectrum can be found by measuring the acollinearity distribution of low-angle Bhabha scatters. Measurement of the acollinearity of pairs observed above 10 degrees polar angle needs to

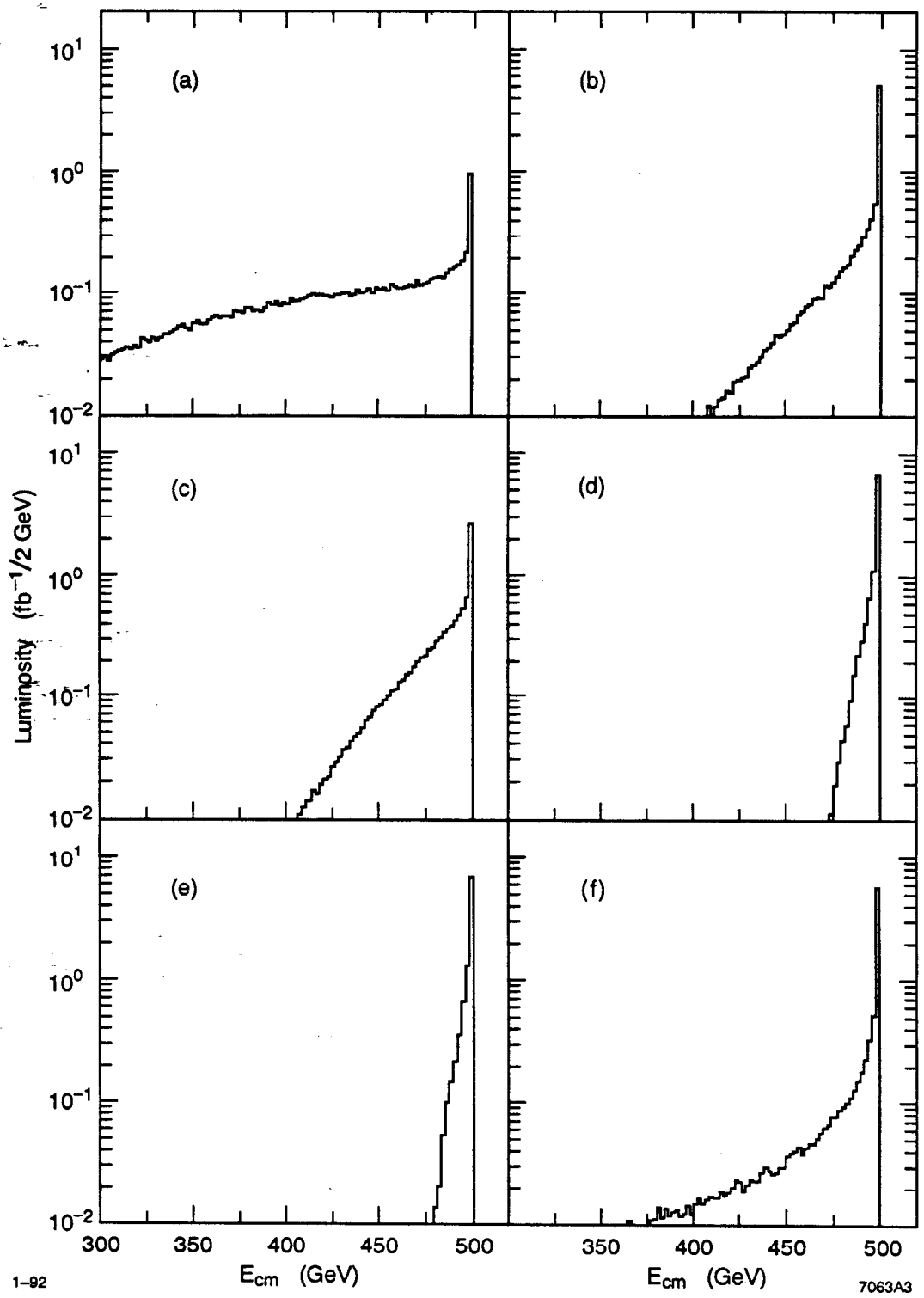


**Figure 7.** Comparison of initial-state radiation and beamstrahlung spectra. (a)-(e) Center of mass energy in various machine designs; (f) smearing of $E_{cm}$ due to initial-state radiation. The intrinsic energy spread of the beam created by the linac (typically 0.2%) has not been included in any of these plots.

be done with a precision of 1 mr in order to reconstruct the center of mass energy with a precision of 1 part in 1000.

## 2. Backgrounds at Linear Colliders

### *2.1. Introduction*

While the physics environment created by electron-positron annihilation is remarkably neat and orderly, the single-pass nature of a linear collider poses a very special challenge to the experimenter and machine designer. Unlike a storage ring in which the circulating beam is quickly reduced to only those particles that are well-contained within the phase space of the physical and dynamic apertures of the machine, a pulsed collider will transmit particles that are very near to its aperture limit. Such particles will create backgrounds in experimental detectors either through the emission of synchrotron radiation as they pass through magnetic fields near the detector, or by the creation of secondary debris when they strike physical elements along the beamline. It is important for the detector to be properly masked, and for the beam to be properly collimated to remove beam extremeties, or "tails," well upstream of the interaction region.

A quantitative sense of the background problem can be gained by comparing the rates at which particles are lost from beams stored in rings with a similar quantity at a linear collider. The beam stored in a ring typically consists of $10^{10}$ particles per bunch, and the bunches pass through the detector with a frequency of a megahertz or so. A beam lifetime of several hours corresponds to a loss of less than one particle per turn per bunch in the ring. The beam in a linear collider also consists of about $10^{10}$ particles per bunch, but it is difficult to avoid losing a few per cent of the beam during the acceleration and focusing processes. (*I.e.*, an "injection efficiency" of 99% would be a good performance figure.) This means that at least $10^8$ particles are being lost per pulse per bunch—this is the source that must be effectively contained by the design of the machine, collimation of the beam, and the design of the masking and choice of components for the detector.

The experience of the Mark II and SLD detectors[10] at the SLC has been an invaluable guide to the problems that will be encountered by experiments at future linear colliders. An example is provided by the first hadronic $Z^0$ decay observed by the Mark II (Fig. 8). In addition to the tracks left by the products of the decay of the $Z^0$, the detector suffers from noise in the drift chamber and time-of-flight counters created by synchrotron radiation created in the final quadrupole lenses of the machine. Penetrating muons and soft electromagnetic debris created by high energy electrons and positrons that have been lost from the machine aperture also contribute to the background in the detector. The high-energy electrons and positrons that create these backgrounds may already be secondary (or even tertiary) debris created by a parent beam particle that went astray still further upstream.

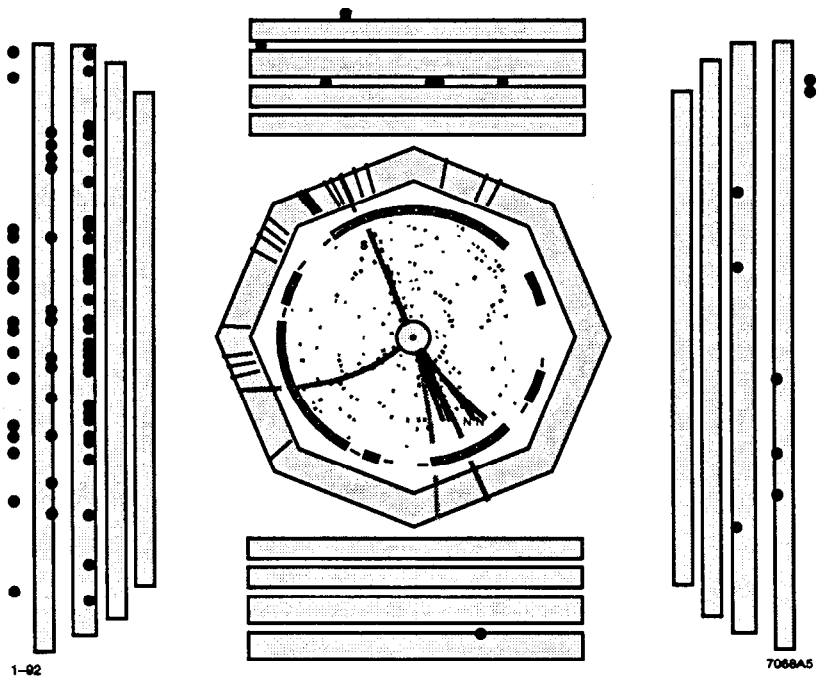

**Figure 8.** The first hadronically decaying $Z^0$ observed by the Mark II at the SLC.

We will discuss these various machine-induced backgrounds in the remainder of this section. Particular use will be made of the SLC experience.

### *2.2. Synchrotron Radiation*

To generate sufficient luminosity to do physics at linear colliders it is necessary to strongly focus the beams to small transverse dimensions at the interaction point of the machine (Fig. 9). The angular divergence of the beam and the lowest-order monochromatic spot size are given in terms of the beam emittance $\epsilon$ and machine $\beta$-function by,

$$\theta^{*^2} = \epsilon/\beta^*$$

$$\sigma^{*^2} = \epsilon \cdot \beta^* \quad .$$

These can be combined to give,

$$\sigma^* = \epsilon/\theta^* \quad .$$

So the luminosity is maximized with the largest $\theta^*$ that can be tolerated before chromatic aberrations begin to dominate the focusing of the beam. An exact calculation[11]

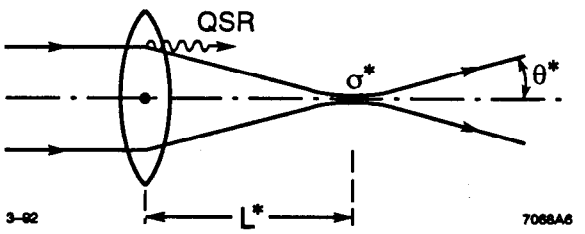


**Figure 9.** Synchrotron radiation in lenses at the interaction region of a collider. Parameters that determine the lowest order geometric size of the electron beam at the interaction point are denoted by a "*".

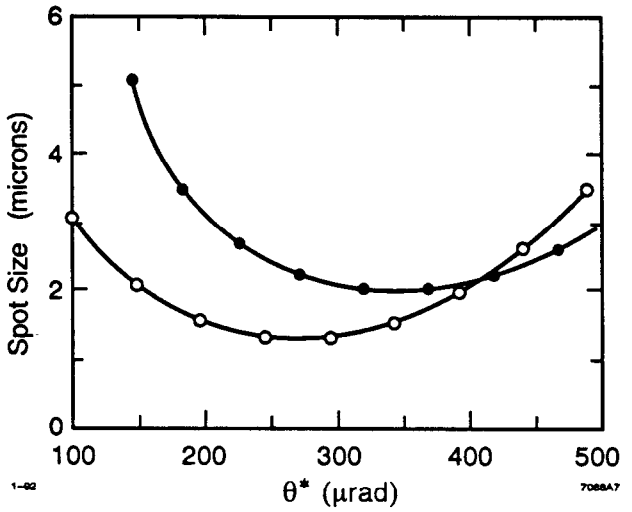


**Figure 10.** The transverse beam size at the SLC interaction point calculated for horizontal (solid points) and vertical (open points) invariant emittances of $5 \times 10^{-10}$ radm and $3 \times 10^{-10}$ radm, respectively.

of the optimal spot size at the SLC interaction point is shown in Fig. 10 for typical operating conditions of the machine during first tests of the SLD. Minimum spot sizes are obtained with angular divergences of 300–350 $\mu$rad, beyond which chromatic aberrations become uncontrollable.

On the other hand, the critical energy of the synchrotron radiation emitted during the focusing process, and the number of photons emitted per path length are given by,

$$k_C = \frac{3}{2} m_e \gamma^3 \left(\frac{\lambda_e}{\rho}\right) \sim \theta^*$$

$$dN_{SR} = \frac{5\alpha}{2\sqrt{3}} \gamma \left(\frac{dl}{\rho}\right) \sim \theta^* \ .$$

It is clear at once that the desire to minimize the flux of synchtrotron radiation passing through the interaction region is in direct conflict with the need to focus the beams to small spots.

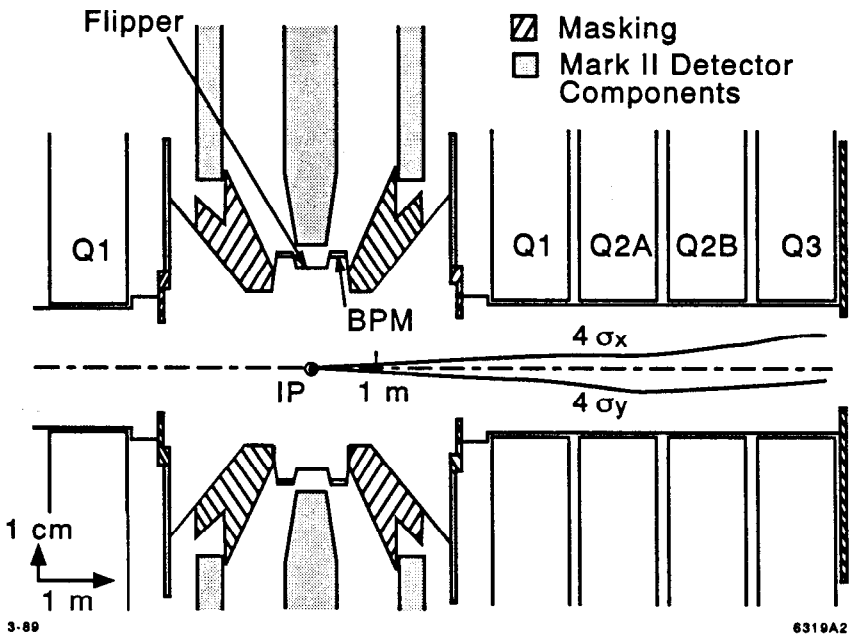


**Figure 11.** Detector masking layout of the Mark II. Particle orbits are shown for four times the nominal angular divergence in the horizontal ($x$) and vertical ($y$) planes.

Most of the photons produced in the final lenses pass directly through the interaction region and exit through the beampipe on the opposite side of the detector. A small fraction, however, are emitted at larger angles and strike the beampipe inside the detector or the face of the opposing quadrupole. An elaborate masking scheme is needed to prevent these photons from flooding the detector elements. The masks and small radius detector elements of the Mark II are shown in Fig. 11. There is no direct path that reaches any detector element that can be taken by a photon emitted along any incoming beam trajectory. Synchrotron photons typically have energies of a few kilovolts, however, and those that strike masking elements rescatter with high probability. The masking is designed to require at lease two scatters before a photon can reach any detector element. (A similar scheme is used for the SLD detector.)

Masking is able to control the background due to photons emitted by the Gaussian core of the beam, but non-Gaussian tails will cause problems. A detailed set of calculations[12] of the background expected in the SLD central drift chamber is given in Fig. 12. The interpretation of this figure is that if the optics of the Final Focus system are set to produce the best possible luminosity (*i.e.*, $\theta^* \approx 300$ $\mu$rad), then the beam "tail" beyond 4–5$\sigma$ of the nominal beam core must be effectively eliminated. To achieve this requires careful control of the beam during acceleration and tight collimation of the beam well upstream of the detector. The hardware used to collimate the beam at the SLC (described below) is not perfect, but it does provide apertures that can be set and maintained near the nominal beam size. Data taken with the SLD are shown in Fig. 13. The amount of background seen in the detector is low

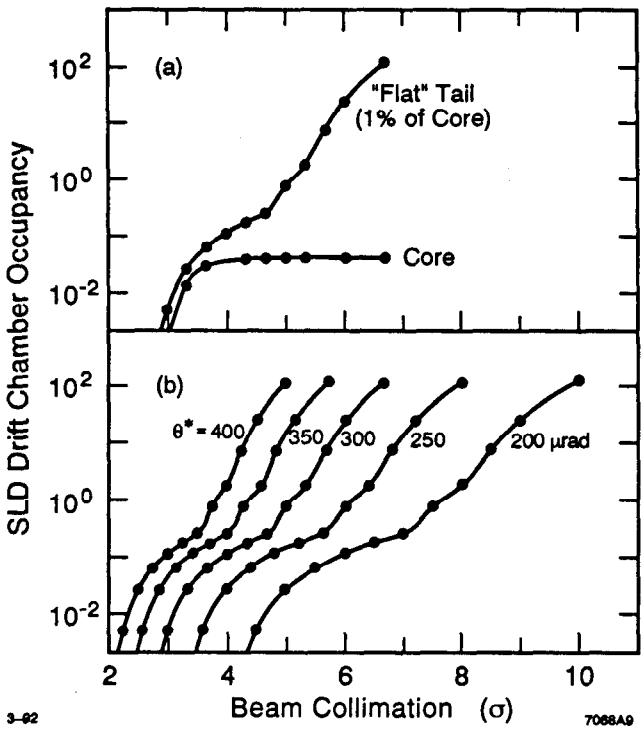


**Figure 12.** Monte Carlo calculation of synchrotron backgrounds in the SLD central drift chamber. The vertical axis is the number of synchrotron photons that create a secondary charged particle in the detector normalized to the total number of signal wires in the detector. It is approximately the fraction of signal wires that would be read out on each machine pulse. The horizontal axis is the maximum extent of phase space occupied by any beam particle as it passes through the final quadrupole lenses. (a) Background created by a beam core of $5 \times 10^{10}$ particles with design emittance, and by a non-Gaussian "tail" containing 1% of the beam core. The beamline is assumed to be adjusted to produce an angular divergence of 300 $\mu$rad for the beam core. (b) Dependence of the background created by the beam "tail" as the focusing ($\theta^*$) of the beam core is varied.

until $\theta^*$ is increased beyond 300 $\mu$rad, at which point it sharply rises. This behaviour is quite consistent with what is expected (Fig. 12).

### *2.3. Interaction Region Design and Synchrotron Radiation at Future Colliders*

Clearly the design of the interaction region of the machine is an important factor in the dynamics that create backgrounds in the detector. At future machines there will be additional constraints on this design beyond the interplay between backgrounds and luminosity that have been encountered at the SLC. If the collider is designed to operate with a large number of closely spaced bunches (*e.g.*, machines based on X-Band rf), or if the beam-beam interaction results in a large disruption of the beam, then it is likely to be necessary to collide the beams at a finite crossing angle. The "crab-crossing" technique[13] illustrated in Fig. 14 can be used to assure

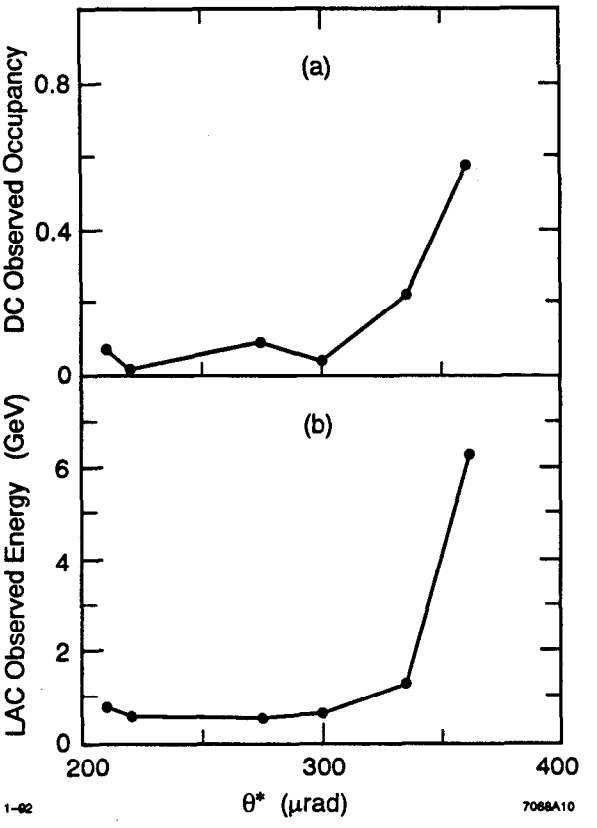


**Figure 13.** Backgrounds observed in the SLD detector at differing values of $\theta^*$. The beam contains $3 \times 10^{10}$ particle per pulse, and the primary collimation of the beam is set at four times the nominal sigma of the beam at each of two betatron phases. (a) Central drift chamber occupancy. (b) Energy deposited in the liquid argon calorimeter.

that the bunches pass completely through each other. The crossing angle allows the disrupted beams to exit the interaction region through openings in the profile of the final quadrupoles that are larger than the aperture between the pole tips seen by the incoming beam. Several possible arrangements are shown in Fig. 15.

Most of the synchrotron radiation emitted in the final quadrupole lenses will follow the beam trajectory and pass through the large exit hole on the downstream side of the interaction region. Some photons, however, are emitted at large angles and will strike the smaller apertures of the focusing lenses themselves. These photons can be scattered into the detector. To reduce the background seen in the detector to acceptable levels, it is still necessary to carefully collimate the "tails" of the beam phase space and to properly mask the detector from the sources of radiation.

An example is provided by a calculation made[14,15] of the radiation pattern produced in the final quadrupoles of the Final Focus system of the Japan Linear Collider (JLC). The result is given in Fig. 16 with differing assumptions for the incoming beam profile. For comparison, the simple masking design shown in Fig. 17 was used

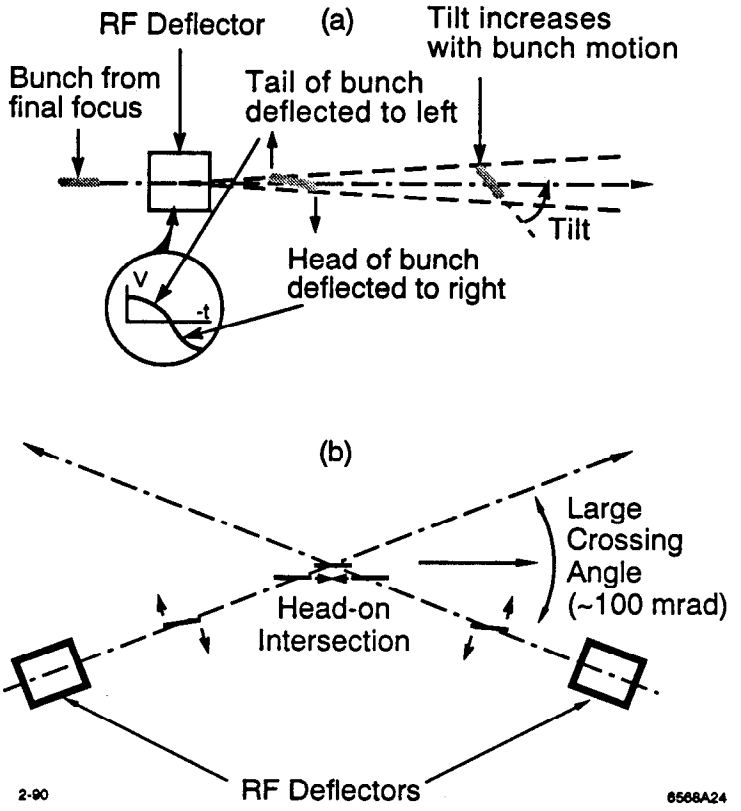


**Figure 14.** "Crab-crossing" layout of the interaction region of a linear collider. The crossing angle can be adjusted to be a few milliradians up to as much as 100 mrad with reasonably sized cavities.

to estimate the maximum flux that can be allowed to strike the quadrupole aperture before the detector is rendered useless. The aperture of the final quadrupole is typically between 0.5 and 1 mm, so the problem is similar to that encountered at the SLC. It will be necessary to collimate beam "tails" beyond 5 or 6 times the nominal beam size.

### *2.4. Collimation of High Energy Electron Beams*

While careful control of the dynamics of the beam during production and acceleration can minimize the number of particles that populate the extremeties of phase space, we can expect that it will always be necessary to collimate the fully accelerated beam. This requires the design and fabrication of systems of collimators that are able to absorb high power densities from errant beam pulses, yet be "black" enough to efficiently remove unwanted beam particles from normal pulses.

A limit on the efficiency that can be achieved with a mechanical scraper is set by the regeneration of secondary particles in the scraper itself (Fig. 18). Beam particles

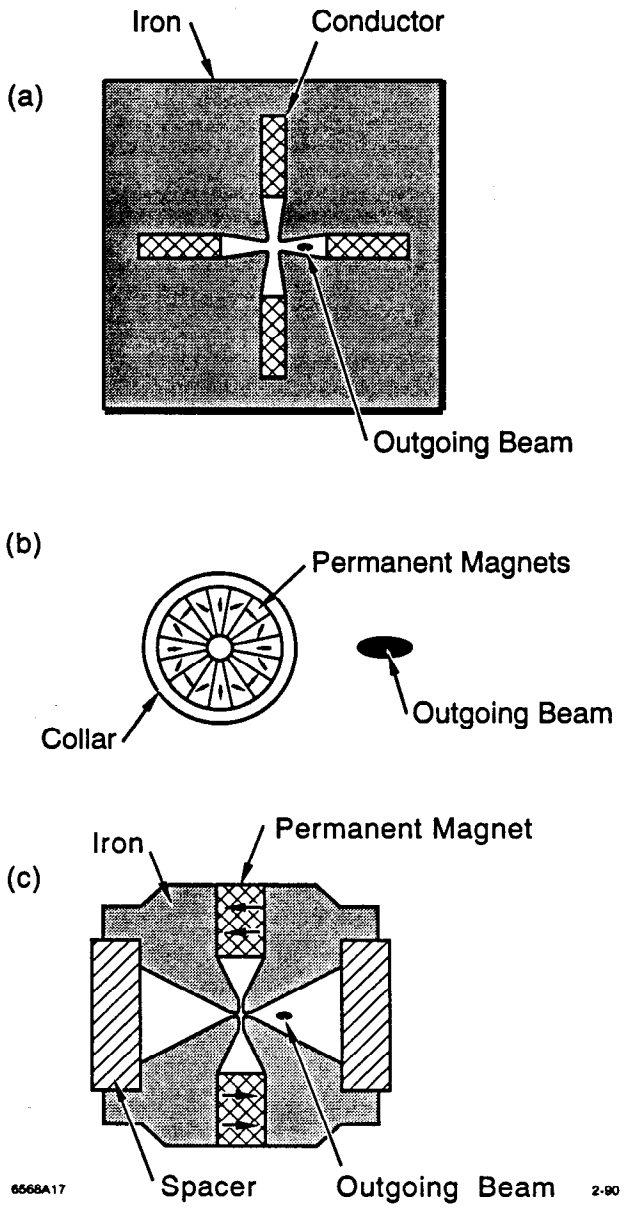


**Figure 15.** Profiles of quadrupole magnets that would allow the disrupted beam to exit the interaction region without striking the pole tips of the lens. The distance between the outgoing beam and the center of the magnet is determined by the focal length of the magnet and the crossing angle of the beams at the interaction point. The point at which the exiting beam would pass by or through the profile of the quadrupole is shown for each case under the assumption of a 100 mrad crossing angle at the interaction point.

that strike the edge of the collimator (or the face of the jaw within 5–10 $\mu$ of the edge) can be scattered back into the aperture of the downstream optical system. Furthermore, since the thickness of the jaw must be kept below a few (typically two) radiations lengths to avoid damage, a percentage of the particles that strike the jaw

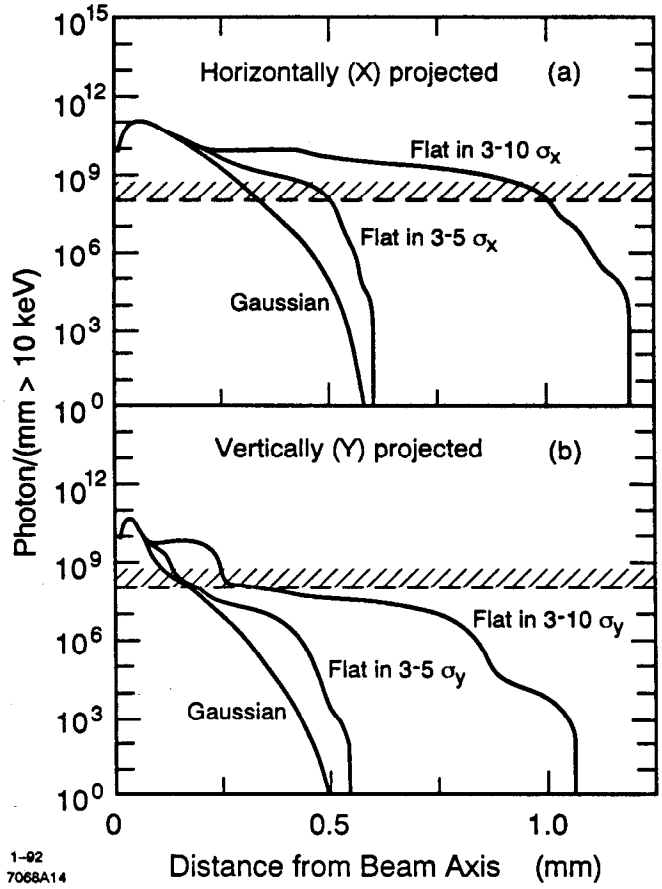


**Figure 16.** Synchrotron radiation profiles at the aperture of the final quadrupole lens for three different beam distributions. Beam "tails" are assumed to be sharply cut off by upstream collimators outside the regions shown in the figure. The estimated limit that can be tolerated by the detector is indicated by the hatched line. The detailed shapes of the profiles are created by the details of the optical design of the final lenses and their aperatures.

will pass through it with insufficient loss of energy to be effectively removed from the beam. As a rule, it is difficult to reduce the flux of unwanted beam particles by more than three orders of magnitude with a single collimation.

Production of pairs of high-energy muons in electromagnetic showers generated when beam particles strike collimator jaws is another, particularly troublesome, background. As we discuss below, this process limits the amount of beam that can be intercepted in the final sections of the machine. It is essential that beam collimation be done far upstream of the detector, and that multiple layers of collimation be used.

The system of collimators used at the SLC is shown schematically in Fig. 19. Primary collimation of each transverse plane is done with pairs of slits situated at points differing by 90 degrees in betatron phase at the end of the linac. The beam is typically 100 $\mu$ in transverse dimension at the point at which it is being collimated,

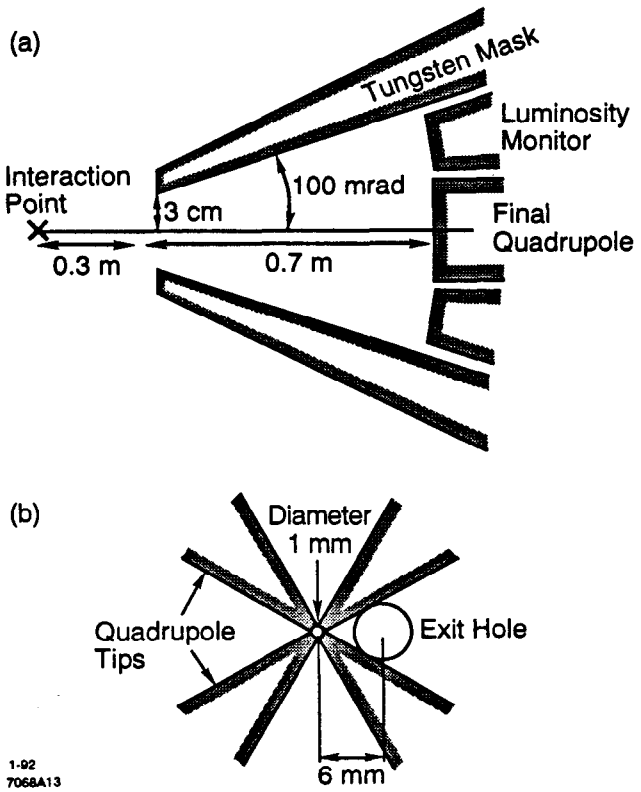


**Figure 17.** Synchrotron radiation profiles at the aperture of the final quadrupole lens for three different beam distributions. Beam "tails" are assumed to be sharply cut off by upstream collimators outside the regions shown in the figure. The estimated limit that can be tolerated by the detector is indicated by the hatched line. The detailed shapes of the profiles are created by the details of the optical design of the final lenses and their aperatures.

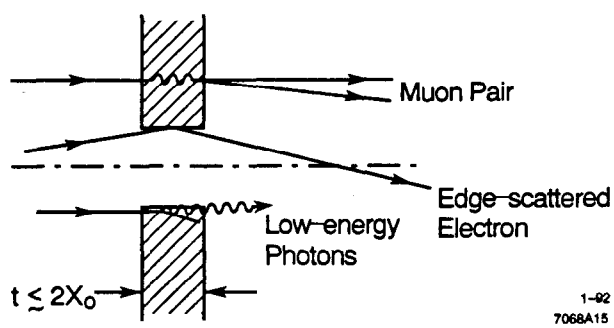


**Figure 18.** Production of secondary particles in a thin collimator.

and its transverse position can be maintained to within 50 $\mu$ of a desired location. The slits are constructed from titanium jaws 2 radiation lengths thick that are capable of being positioned to within 20 $\mu$ of a desired aperture. Secondary collimators in the Arc transport lines are used to clean up debris created in the primary slits, and

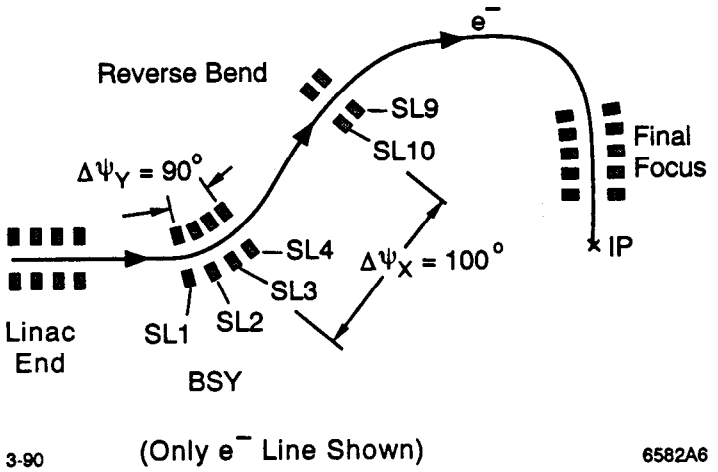


**Figure 19.** Beam collimation at the SLC.

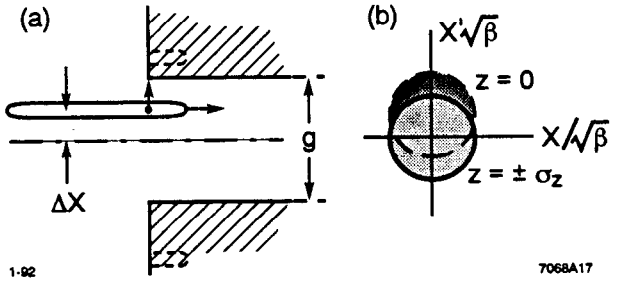


**Figure 20.** Phase space occupied by beam particles after passing off-axis through a narrow collimator aperture. Particles at the ends of the bunch where the density is low receive less kick from geometric wakefields than do particles near the beam center where the density is high.

a third layer of collimation exists in the Final Focus. The apertures of the primary slits are typically set to 4–5 times the nominal beam size, and the subsequent Arc and Final Focus collimators are used with slightly larger settings. Unfortunately the optics of the Arc transport is not ideally suited for this purpose; it is not possible to establish secondary collimation at two betatron phases at points in the beamline that are free of horizontal dispersion. This allows secondaries with the proper correlation between betatron phase and energy offset to slip through the system.

At higher energy machines the problem of beam collimation will become more severe. The beam at the end of the linac will be no more than a few microns in transverse dimension, and the energy in each machine pulse will reach hundreds of Joules. A single pulse may damage even thin scrapers. A further complication arises because of the need to preserve the small emittance of the beam. If the beam is not steered exactly through the center of the aperture of a pair of jaws then the imbalance in the image charge distribution induced in the material of the jaw results in a net force that is excerted on the particles in the beam [Fig. 20(a)]. The kick received by

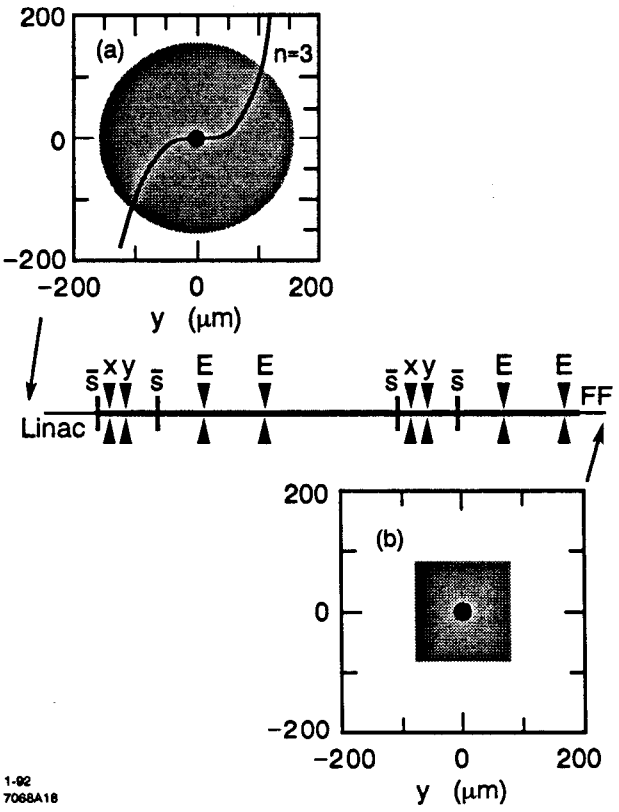


**Figure 21.** Schematic representation of the principle of nonlinear collimation. Scrapers are represented by the symbols $x$, $y$, and $E$, and skew sextupoles are denoted by $\bar{S}$. (a) The beam as it might appear at the input to the collimation section with a central core (black) and an extensive halo (shaded). The relative strength of the sextupole fields in the beamline is indicated by the curve labeled "$n = 3$". (b) The beam after collimation.

each particle is determined[16] by the longitudinal density profile of the beam $q(z)$, the collimator gap $g$, and the offset of the bunch in the gap $\delta x$,

$$\delta\theta(z) \quad \sim \quad q(z)\,\frac{\delta x}{g} \quad .$$

The effect is to shift the regions of transverse phase space occupied by particles in the beam by amounts that depend upon their longitudinal position within the bunch as illustrated in Fig. 20(b).

The increase in the emittance of the beam caused by trajectory errors through collimators with small apertures is found to be unacceptable when the wakefield is correctly evaluated with proper account given to the finite conductivity of the material of the jaw.[17] It may be possible[18] to use sections of beamline specifically designed to include nonlinear magnetic fields to preferentially defocus particles far from the central core of the beam to allow them to be collimated with larger aperture slits.

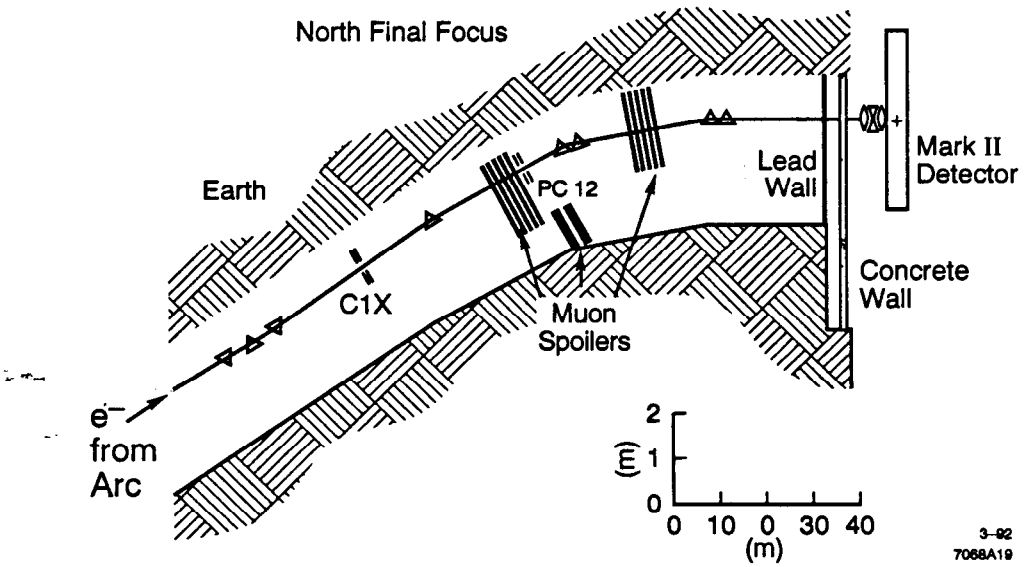


**Figure 22.** Layout of toroidal muon spoilers in the Final Focus tunnel at the SLC. The collimators C1X and PC12 are slits used to shadow the apertures of the final quadrupole lenses shown near the detector.

An example[19] of a section designed to use sextupole fields ($n = 3$) for this purpose is shown in Fig. 21. Particles in the halo that surrounds the beam core are defocused by the sextupole fields in the beamline and then collimated. To avoid unacceptable distortion of the phase space by the nonlinear fields it is necessary to symmetrize the topology of the sextupole magnets by placing them in pairs 180 degrees apart in betatron phase. The resulting mechanical alignment and optical matching tolerances on this section of beamline are similar to those encountered in the Final Focus section of the machine. The problem of beam collimation is sufficiently difficult, however, that it may require that such sections be included in the design of the accelerator.

### *2.5. Muon Backgrounds*

A particular problem that occurs when beam particles are lost or deliberately collimated is the creation of muon pairs through the Bethe–Heitler reaction in electromagnetic showers. These pairs are produced with significant energies and generally at very forward angles. The linear topology of the accelerator and focusing systems is such that many of these penetrating particles will strike the detector at the interaction point, and can cause unacceptable trigger rates and, if allowed to become too severe, loss of efficiency in the detection and reconstruction of particles produced in real electron-positron annihilation events.

To control this problem at the SLC it was found to be necessary to install large toroidal magnets around the beamline to provide deflecting fields for particles travel-

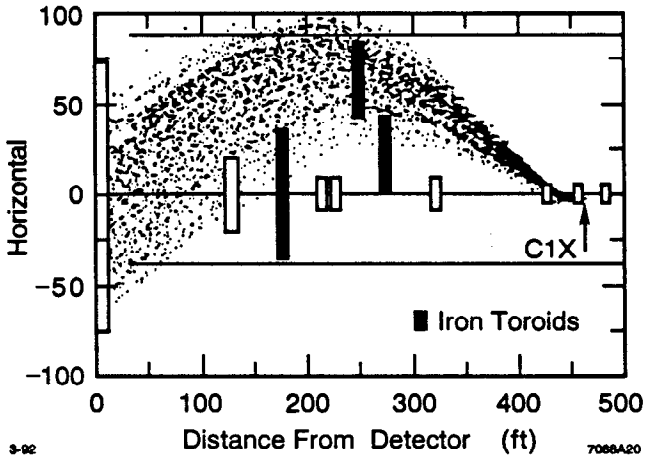


**Figure 23.** Trajectories of muons created in the collimator C1X that would reach the detector in the absence of toroidal fields.

ling outside the beampipe. The layout of toroids in the SLC tunnel, shown in Fig. 22, was designed with the aid of a Monte Carlo simulation[20] that tracks muons through the magnetic fields and materials present in the tunnel. Examples of tracks that reach the detector are shown in Fig. 23, and calculated background rates are summarized in Fig. 24. The muon flux that reaches the detector varies from $10^{-5}$ to $10^{-6}$ per electron lost in the Final Focus in the absence of the muon spoilers. The addition of the toroids reduces the muon flux by about one order of magnitude for losses on the most upstream beamline elements. During normal SLC operation it is typical to find $10^7$ beam particles striking apertures at the entrance to the Final Focus, and considerably less striking apertures closer to the interaction point. The rate and azimuthal distribution of muons passing through the detector was measured[10] with the Mark II to be completely consistent with the predictions of the Monte Carlo and the estimated loss of beam on various apertures. The toroids in the SLC Final Focus have proven to reduce the muon flux sufficiently well to avoid problems with data acquisition and analysis, but the beam orbit through the Final Focus must be carefully maintained to avoid significant increases in the loss of beam.

A schematic layout of the final sections of a future linear collider, shown in Fig. 25, includes a final section of beam collimation followed by a set of toroid muon spoilers similar to those used in the SLC. It is possible to bend the beam through an angle of 10 mrad or so in a tightly focused lattice (similar to the Arc regions of the SLC) to minimize the number of muons that reach the detector. This bend is probably necessary. Detailed calculations[21] of the muon background have been made for the specific layout shown in Fig. 26. The results are given in Fig. 27. The solid angle of the detector as seen from the beginning of the Final Focus is reduced as the energy is increased (compare the length of the Final Focus beamlines in Figs. 22 and 26), but the muon production rates and peak energies are correspondingly increased and the production angles are reduced. The result is that the number of muons that reach the detector per electron lost in the Final Focus region remain nearly the same as those

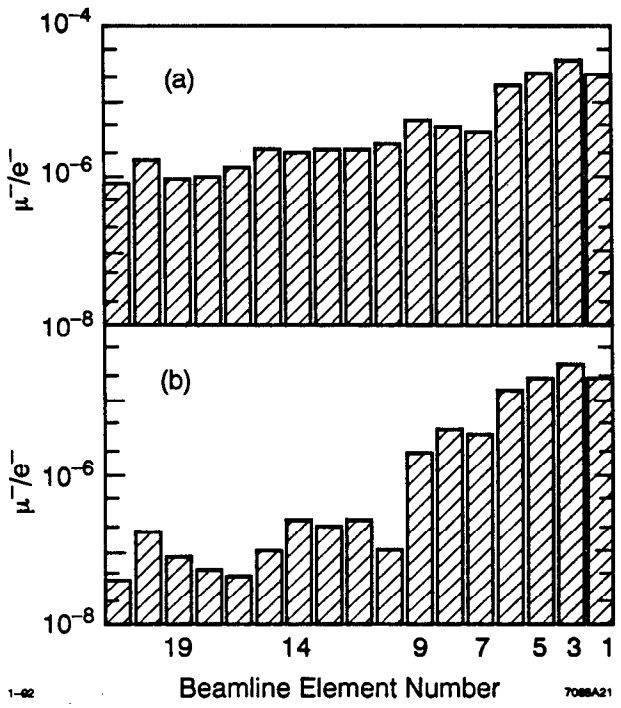


**Figure 24.** Calculated background rates for muons in the Mark II detector for electrons targeted onto various beamline elements. The vertical scale is the number of muons that reach the detector per incident electron. The collimator C1X is element number 16 and the smaller numbered elements are closer to the detector. (a) Without muon spoilers. (b) With the spoilers shown in Fig. 22.

experienced at the SLC. It was found in this simulation that if the total bend angle between the end of the linac and the interaction region is increased from the 4.2 mrad needed for the chromatic correction of the Final Focus optics to 12.6 mrad, then the muon background is reduced by a factor of 10. The conclusion is that isolation of the detector from the beam of muons created in the linac and collimation sections of future colliders will likely require sections of beamline designed to bend the electron beam through significant angles and to allow room for the installation of magnetic elements and shielding to deflect and absorb high energy muons.

## 3. Backgrounds from the Beam-Beam Interaction

So far we have discussed backgrounds that are created by each beam as it traverses the beamline leading to the interaction point of the collider. There are also a number of backgrounds that can be created by the interaction of the two beams. The underlying source of this problem can be traced to the fact that the luminosity *per machine pulse* becomes extremely high in many collider designs. The luminosity required to study electron-positron annihilation physics is $10^{33}$ cm$^{-2}$ s$^{-1}$ at 500 GeV center of mass energy. With machine repetition rates of 100 to 1000 cycles per sec-

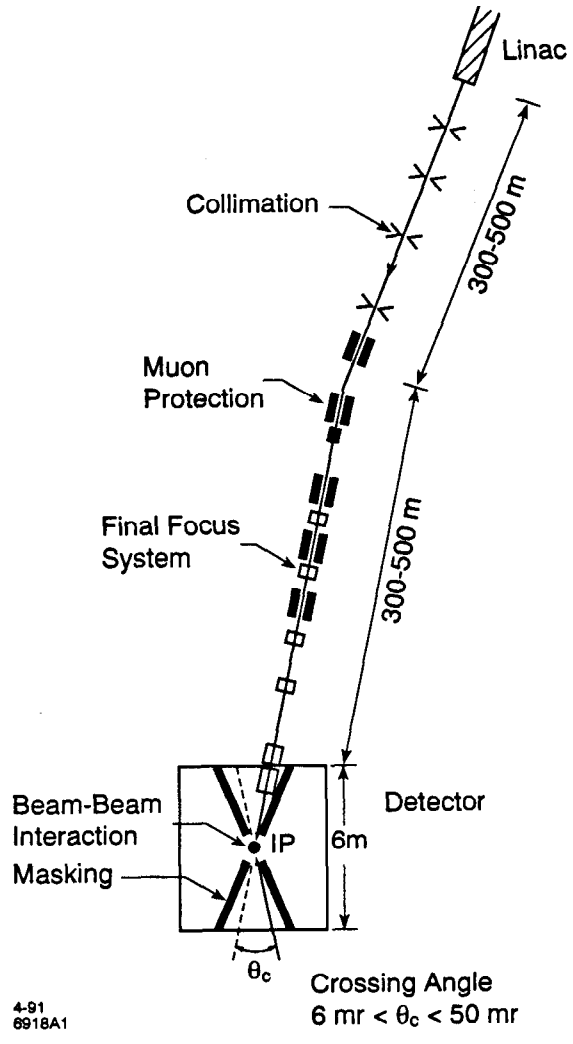


**Figure 25.** Schematic layout of the final sections of a linear collider.

ond, the luminosity per machine pulse becomes $10^{30}$–$10^{31}$ cm$^{-2}$. The accompanying Weizäcker–Williams photon-photon luminosity is similarly large, and the $\gamma\gamma$ cross sections are huge (see Table V). For example, the total cross section for the reaction,

$$e^+e^- \rightarrow e^+e^-e^+e^-$$

is of order $10^{-26}$ cm$^2$ at high energies. There will be $10^4$–$10^5$ secondary electron-positron pairs produced on each machine pulse! The problem is made worse by the enhanced flux of photons created by the beamstrahlung process,[8] and by the strong electromagnetic fields in the colliding bunches.

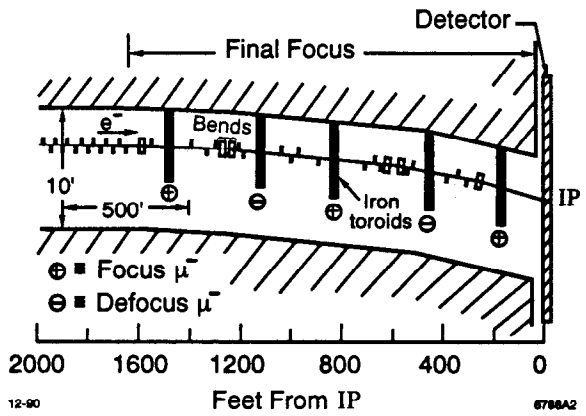


**Figure 26.** Schematic of the Final Focus beam line used[21] to study the background of muons in detectors at a 0.5 TeV linear collider.

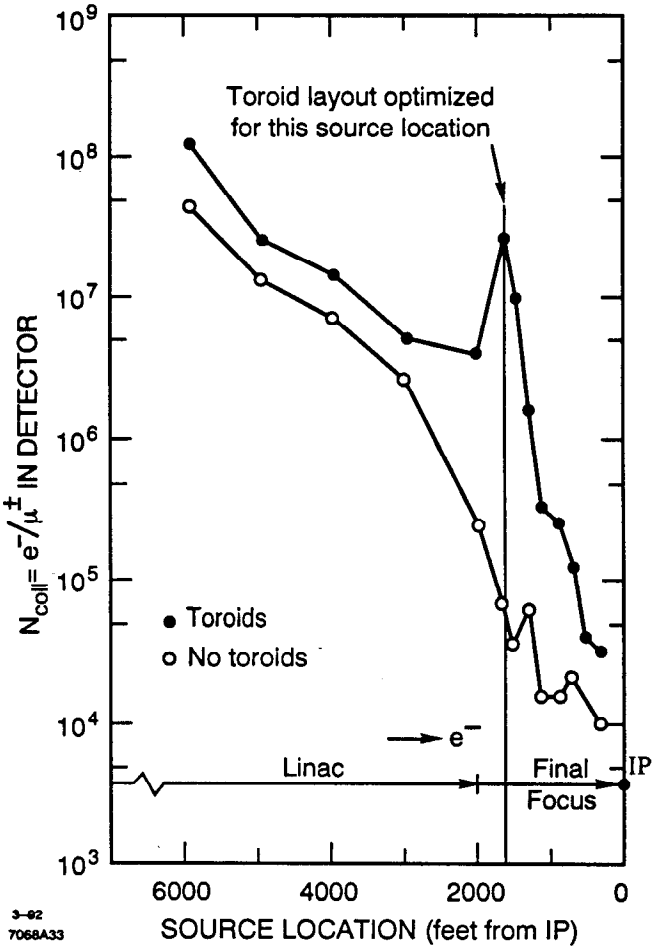


**Figure 27.** Estimated[21] number of electrons impinging on a collimator which yield one muon in the detector as a function of source location in the linac and Final Focus of the layout shown in Fig. 26.

A number of interactions can cause undesirable backgrounds in detector elements,

| | | |
|---|---|---|
| $\gamma e$ | $\rightarrow e^+e^-e$ (Bethe–Heitler) | Incoherent pair production |
| $\gamma\mathcal{EM}_{coherent}$ | $\rightarrow e^+e^-$ (Schwinger) | Coherent pair production |
| $\gamma\gamma$ | $\rightarrow l^+l^-$ | |
| | $\rightarrow hadrons$ | (Landau–Lifshitz) |

The dominate reactions are those that produce electrons and positrons in the final state. These all proceed with large cross sections, but most of the rate occurs at small invariant masses and at very forward polar angles. Further, the coherent (Schwinger) pair-production process can be controlled by avoiding machine designs with large disruption parameters. As a result, most of the particles that are produced do not directly generate backgrounds in detector elements that surround the interaction region. The flux of particles that strike the surfaces of the final quadrupole lenses and synchrotron masking can be large enough, however, that detailed calculations are necessary to determine the rate of secondary scatters that send particles into the detector volume. The influence of the electromagnetic field created by the opposing bunch on the trajectories followed by low-energy electrons and positrons can not be ignored in these calculations.

The trajectories followed by particles created in the beam-beam interation depend on their electric charge as shown in Fig. 28. The magnetic field produced by each bunch focuses opposite-sign particles moving against it, and defocuses like-sign particles. The bunch intensity and size are limited, however, and so there is a maximum transverse momentum that can be generated by this acceleration mechanism. For typical machine designs this maximum occurs at a few tens of MeV, so most particles are contained by the solenoidal magnetic field of the detector and exit the interaction region at small radii. Designs that incorporate a small crossing angle (Fig. 14) are beneficial since nearly all high-energy particles created at the interaction point will pass through the large exit holes intended for the disrupted beams and synchrotron radiation. The residual background due to particles backscattered into the detector has been evaluated[14,15] using the masking design shown in Fig. 17, and found to be quite small—well below the background due to synchrotron radiation created by even a small beam tail. These calculations, however, have ignored the finite momentum transfer that occurs in the fundamental processes themselves. While this is generally low, there is a finite probability to produce an electron-positron pair with large invariant mass. Corrections for this effect as well as improvements in the tracking of particles through the complex fields of the beam-beam interaction are presently being incorporated into the Monte Carlo simulations.[22]

The production of hadronic final states by the interactions of photons occurs with a much smaller cross section than purely QED reactions, but these processes

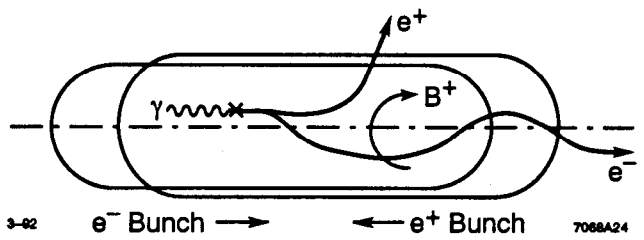


**Figure 28.** Trajectories of low-energy electrons and positrons created in the beam-beam interaction. The positron bunch creates the magnetic field $B^+$ in the laboratory frame of reference.

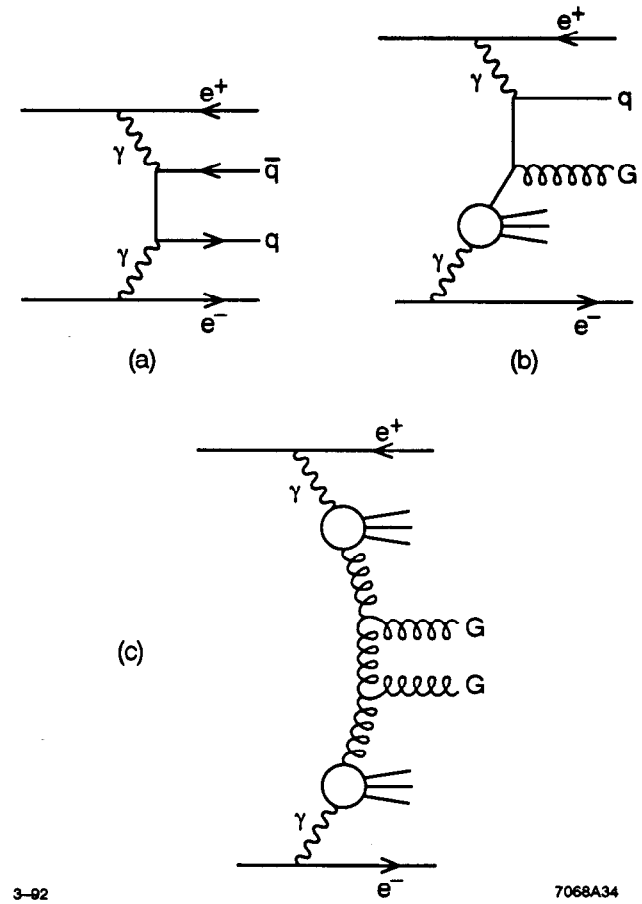


**Figure 29.** Photon-photon reactions in the model of Reference 23. (a) Direct hard-scattering, (b) "once-resolved" reactions, and (c) "twice-resolved" reactions.

are characterized by a considerably larger range of invariant masses and transverse momenta. The photon acts as a source of partons in much the same way that a proton does. The hadronic structure function of the photon has not been fully measured, but the Vector Meson Dominance (VMD) model is probably a good description of photon-photon collisions at low $Q^2$. In this case, the photon can be thought of as a pair of

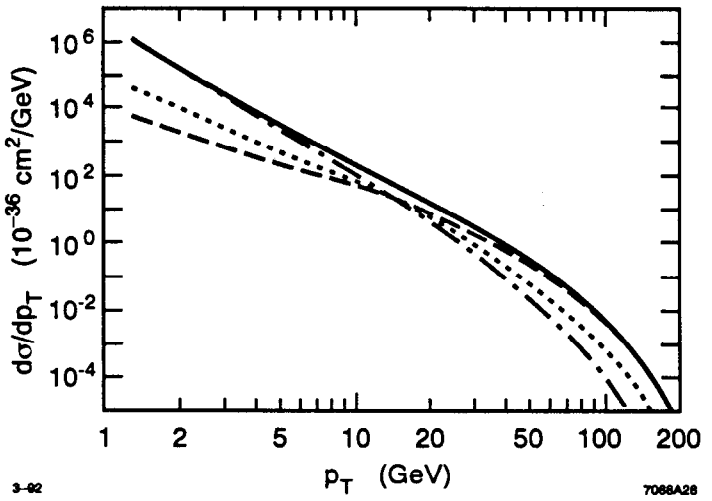


**Figure 30.** "Minijet" production cross sections for the various processes shown in Fig. 29. Direct hard-scattering rates indicated with a dashed line, "once-resolved" rates are given with the dotted line, and the dashed-dot curve is the rate for "twice-resolved" processes. The solid curve is the incoherent sum of the three contributions.

quarks that are strongly bound into a vector meson. Collisions are predominantly forward-peaked diffractive processes. At very high momentum transfer, the photon behaves as a point particle to create a quark-antiquark pair that then fragment into hadrons. This process can create jets of hadrons at large transverse momentum, but the cross section is low.

The structure of the photon at moderate values of $Q^2$ is not known well at all. One calculation of the probablility that a photon will be resolved into a quark or gluon with significant momentum fraction has been presented at this conference.[23] Photon-photon collisions are allowed to proceed through the "once-resolved" and "twice-resolved" reactions shown in Fig. 29. The contributions of these reactions are adjusted to fit recently presented data.[24] The "once- and twice-resolved" processes give rise to large cross sections for the production of "minijets" with transverse momenta of tens of GeV. The results of the calculations are shown in Fig. 30. While the direct Born production of quark pairs is well below a rate that is worrisome, the gluon content of the photon in this model is sufficiently large that minijets with 1–2 GeV of transverse momentum are predicted to be created by gluon-gluon collisions with sizable cross sections.

It should be emphasized that the existence of the "resolved" processes that dominate the "minijet" production cross section is not firmly established. On the other hand the hadronic photon-photon cross section surely contains a piece described by the Vector Dominance Model which can not be ignored. As summarized in Table V, this cross section will be of order $10^{-30}$ cm$^{-2}$, close to the luminosity per machine pulse. The events that are produced will be sharply peaked at low invariant masses,

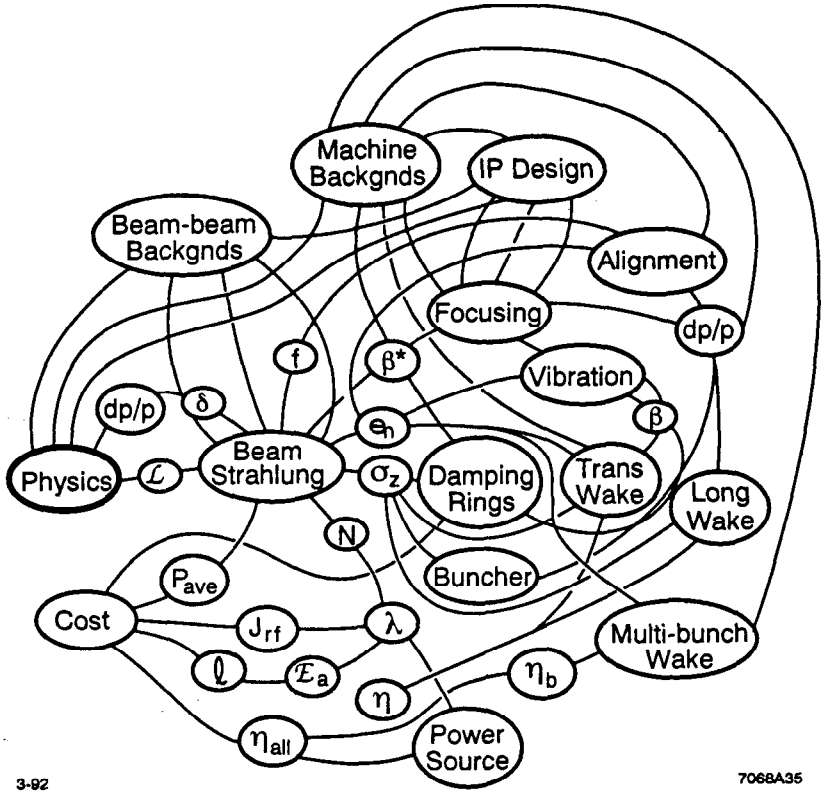


**Figure 31.** Programatic view of connections and constraints in the design of linear colliders.

and it is not clear at this time what effect, if any, they will have on analysis of annihilation events.

## 4. Experimentation and Accelerator Design

Our experience with the SLC and our considerations of what can be expected at future machines has taught us that the problems of accelerator physics and particle physics are inextricably linked. The interplay, shown[25] in *simplified* form in Fig. 31, reaches to the fundamental choices that must be made in the design and implementation of linear colliders and experimental detectors. It is more important than ever that particle physicists and accelerator physicists work together to achieve solutions that provide the energy and luminosity for the next step in $e^+e^-$ colliders without compromise to its particle physics goals.

## References


1. P. Grosse-Weismann, private communication.
2. C. Ahn et al., SLAC-REPORT-329 (1988).
3. T. Barklow, *Proceedings of the Workshop on Physics and Experiments with Linear Colliders,* Saariselkä, Finland, 1991.
4. M. Tigner, *Proceedings of the Workshop on Physics and Experiments with Linear Colliders,* Saariselkä, Finland, 1991.
5. K. Yokoya, *Proceedings of the Workshop on Physics and Experiments with Linear Colliders,* Saariselkä, Finland, 1991.
6. R. Ruth, *Proceedings of the Workshop on Physics and Experiments with Linear Colliders,* Saariselkä, Finland, 1991.
7. C. Adolphsen, private communication, to be published.
8. T. Barklow, P. Chen, and W. Kozanecki, SLAC-PUB-5718 (1991).
9. D. Miller, *Proceedings of the Workshop on Physics and Experiments with Linear Colliders,* Saariselkä, Finland, 1991.
10. R. Jacobsen et al., SLAC-PUB-5205 (1990).
11. K. Brown, private communication.
12. S. Hertzbach, R. Kofler, and T. Maruyama, private communication; see also Ref. 10.
13. R. Palmer, *Proceedings of the 1988 DPF Summer Study, Snowmass '88,* Snowmass, CO, 1988; SLAC-PUB-4707 (1988).
14. T. Tauchi et al., *Proceedings of the First Workshop on Japan Linear Collider,* S. Kawabata (ed.), 1989.
15. T. Tauchi et al., *Proceedings of the 1990 DPF Summer Study on High Energy Physics: Research Directions for the the Decade,* Snowmass, CO, 1990.
16. K. Bane and P. Morton, SLAC-PUB-3983 (1986).
17. K. Yokoya, CERN SL/90-88(AP) (1990).
18. N. Merminga and R. D. Ruth, "Dynamic Collimation for Linear Colliders," *Proceedings of the 1990 EPAC Conference,* Nice, p. 1738; SLAC-PUB-5265 (1990).
19. N. Merminga, J. Irwin, R. Helm, and R. D. Ruth, SLAC-PUB-5507 (1991).
20. G. Feldman, private communication; see also Ref. 10.
21. L. P. Keller, "Calculation of Muon Background in a 0.5 TeV Linear Collider," *Proceedings of the DPF Summer Study on High Energy Physics: Research Directions for the Decade,* Snowmass, CO, 1990.

22. P. Chen, T. Tauchi, and D. Schroeder, "Pair Creation at Large Inherent Angles," *Proceedings of the DPF Summer Study on High Energy Physics: Research Directions for the Decade,* Snowmass, CO, 1990.

23. M. Drees and R. Godbole, *Proceedings of the Workshop on Physics and Experiments with Linear Colliders,* Saariselkä, Finland, 1991; see also Phys. Rev. Lett., **67** (1991) 1189.

24. AMY Collaboration, KEK Preprint 91–14 (1991); Y. Sugimoto, *The Second KEK Topical Conference on $e^+e^-$ Collision Physics,* Tsukuba, Japan, 1991.

25. This figure is a modification of one given by R. Palmer, Ann. Rev. Nucl. Part. Sci. **40** (1990) 529.